Ketamine, but not the NMDA Receptor Antagonist Lanicemine, Increases Prefrontal Connectivity in Depressed Patients

Image Processing

The Human Connectome Project (HCP) Pipelines (github.com/Washington-University/Pipelines) were adapted to process the imaging data [1]. Briefly, the adapted minimal preprocessing included FreeSurfer automatic segmentation and parcellation of high resolution T1 MRI scans, deletion of first 5 volumes, slice timing correction, motion correction, intensity normalization, brain masking, and registration of fMRI images to structural MRI and standard template, while minimizing smoothing from interpolation. Then, the cortical gray matter ribbon voxels and each subcortical parcel were projected to a standard Connectivity Informatics Technology Initiative (CIFTI) 2mm grayordinate space. ICA-FIX was run to identify and remove artifacts [2, 3], followed by mean grayordinate time series regression (MGTR; which is comparable to global signal regression in volume data). The latter two processing steps (FIX+MGTR) have been found to significantly reduce motion-correlated artifacts [4]. In addition, there were no differences in head motion during *f*MRI session between groups at any study time point (see Table S1).

Details of global brain connectivity with global signal regression (GBCr) methods were previously described [5-16]. Briefly, time series were demeaned and normalized, followed by generating dense connectomes correlating each vertex/voxel with all other vertices/voxels in the CIFTI grayordinates, and then transformed to Fisher z values. For each vertex/voxel, GBCr is calculated as the standardized average (z-scored) across those Fisher z values, which generates a map for each *f*MRI session where each vertex/voxel value represents the functional connectivity strength of that grayordinate with the rest of the brain. In graph theory terms, GBCr (also known as Functional Connectivity Strength; FCS [17]) is considered a weighted measure of nodal strength of a voxel in the whole brain network – determining brain hubs and examining the coherence between a local region and the rest of the brain [18].

Similar to previous studies [5], we have limited our investigation to the prefrontal cortex (PFC), 1st because of its critical role in depression, 2nd because previous findings of reduced GBCr were limited to the PFC, and 3rd to limit Type I & Type II errors and facilitate the interpretation of the findings. GBCr maps were smoothed (sigma = 4) prior to vertex-wise analyses. The HCP multi-modal parcellation (MMP) [19] was used to create the PFC mask (delineated in Fig. 2 & 3). Each PFC mask included the following regions: R_FEF_ROI, R_PEF_ROI, R_55b_ROI, R_SFL_ROI, R_SCEF_ROI, R_6ma_ROI, R_33pr_ROI, R_a24pr_ROI, R_p32pr_ROI, R_a24_ROI, R_d32_ROI, R_8BM_ROI, R_p32_ROI, R_10r_ROI, R_47m_ROI, R_8Av_ROI, R_8Ad_ROI, R_9m_ROI, R_8BL_ROI, R_9p_ROI, R_10d_ROI, R_8C_ROI, R_44_ROI, R_45_ROI, R_47l_ROI, R_a47r_ROI, R_6r_ROI, R_IFJa_ROI, R_IFJp_ROI, R_IFSp_ROI, R_IFSa_ROI, R_p9-46v_ROI, R_46_ROI, R_a9-46v_ROI, R_9-46d_ROI, R_9a_ROI, R_10v_ROI, R_a10p_ROI, R_10pp_ROI, R_11l_ROI, R_13l_ROI, R_OFC_ROI, R_47s_ROI, R_6a_ROI, R_i6-8_ROI, R_s6-8_ROI, R_FOP4_ROI, R_AVI_ROI, R_FOP1_ROI, R_25_ROI, R_s32_ROI, R_pOFC_ROI, R_FOP5_ROI, R_p10p_ROI, R_p47r_ROI, R_a32pr_ROI, R_p24_ROI, L_FEF_ROI, L_PEF_ROI, L_55b_ROI, L_SFL_ROI, L_SCEF_ROI, L_6ma_ROI, L_33pr_ROI, L_a24pr_ROI, L_p32pr_ROI, L_a24_ROI, L_d32_ROI, L_8BM_ROI, L_p32_ROI, L_10r_ROI, L_47m_ROI,

L_8Av_ROI, L_8Ad_ROI, L_9m_ROI, L_8BL_ROI, L_9p_ROI, L_10d_ROI, L_8C_ROI, L_44_ROI, L_45_ROI, L_47l_ROI, L_a47r_ROI, L_6r_ROI, L_IFJa_ROI, L_IFJp_ROI, L_IFSp_ROI, L_IFSa_ROI, L_p9-46v_ROI, L_46_ROI, L_a9-46v_ROI, L_9-46d_ROI, L_9a_ROI, L_10v_ROI, L_a10p_ROI, L_10pp_ROI, L_11l_ROI, L_13l_ROI, L_OFC_ROI, L_47s_ROI, L_6a_ROI, L_i6-8_ROI, L_s6-8_ROI, L_FOP4_ROI, L_AVI_ROI, L_FOP1_ROI, L_25_ROI, L_s32_ROI, L_pOFC_ROI, L_FOP5_ROI, L_p10p_ROI, L_p47r_ROI, L_a32pr_ROI.

We have used GBCr, instead of GBC without global signal regression (GBCnr), because the study hypotheses were based on previous GBCr findings [5-11, 13, 17], which provided the rationale for the current report and will facilitate the interpretation of the study findings. Of note, in previous studies we found no GBCnr alteration in TRD and ketamine had no effects on GBCnr levels [6]. For completion, we have repeated the vertex-wise analyses in the current study using PFC GBCnr (i.e., without MGTR), which showed no significant effects of ketamine on PFC GBCnr during infusion or 24h post-treatment. The patterns of uncorrected PFC GBCr and GBCnr changes following ketamine are shown in Fig. S1. It is noticeable that 24h post-treatment the PFC GBCnr clusters (mostly increased) appears to largely follow the same pattern of PFC GBCr changes.

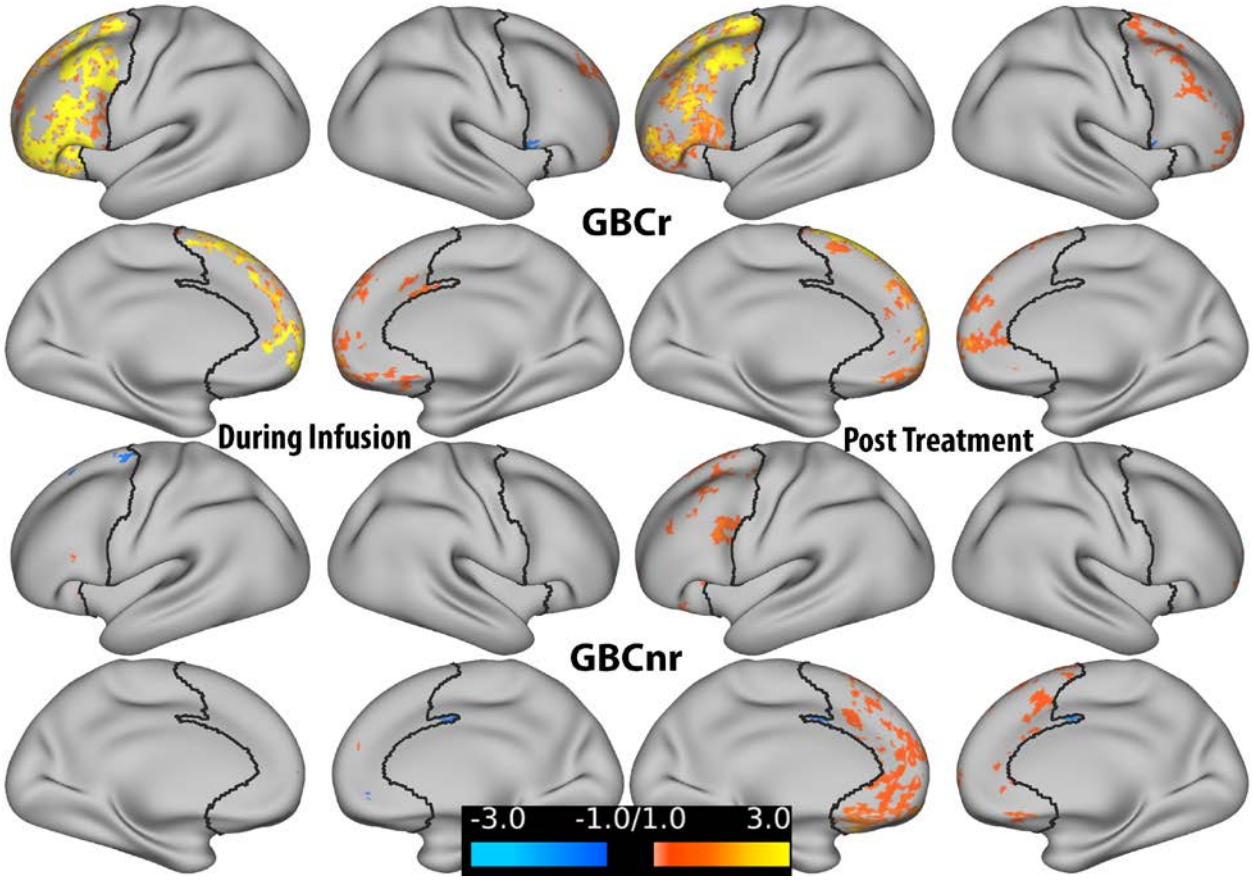

Figure S1. Statistical maps comparing delta PFC GBCr (top) and GBCnr (bottom) between ketamine and placebo. These maps were not corrected for multiple comparisons. None of the clusters in the GBCnr maps will survive correction. Although there were no large GBCnr clusters during infusion (left), it is noticeable that 24h post-treatment the PFC GBCnr clusters (mostly increased) appeared to largely follow the same pattern of PFC GBCr changes (right). The latter observation raises the question whether the higher sensitivity of GBCr is due to its resistance to artifacts.

Table S1. Demographics and Clinical Characteristics

	Placebo	Ketamine	Lanicemine	
	Mean ± *SEM*	Mean ± *SEM*	Mean ± *SEM*	*p*[a]
Subjects (N)	18	19	19	
Female (N; %)	10 (56%)	12 (63%)	12 (63 %)	0.86
Manchester site (N; %)	10 (56%)	9 (47%)	8 (42%)	0.71
Oxford site (N; %)	8 (44%)	10 (53%)	11 (58%)	0.71
Baseline - BDI	26 ± 1.9	31 ± 1.6	34 ± 2.3	0.02
Post-treatment - BDI	18 ± 2.5	22 ± 1.9	26 ± 2.7	0.06
Improvement (%) - BDI	27 ± 8	29 ± 6	20 ± 5	0.49
Baseline – Motion [b]	0.11 ± 0.01	0.12 ± 0.02	0.09 ± 0.01	0.41
During Infusion - Motion [b]	0.18 ± 0.03	0.14 ± 0.01	0.14 ± 0.02	0.46
Post-treatment - Motion [b]	0.12 ± 0.02	0.13 ± 0.02	0.11 ± 0.02	0.52

a. ANOVA or Chi square test (significance set at $p \leq .05$); b. frame to frame motion; **Abbreviations**: BDI: Beck Depression Inventory;

References

1. Glasser MF, Sotiropoulos SN, Wilson JA, et al. The minimal preprocessing pipelines for the Human Connectome Project. *Neuroimage*. 2013; 80: 105-24.
2. Salimi-Khorshidi G, Douaud G, Beckmann CF, Glasser MF, Griffanti L and Smith SM. Automatic denoising of functional MRI data: combining independent component analysis and hierarchical fusion of classifiers. *Neuroimage*. 2014; 90: 449-68.
3. Griffanti L, Salimi-Khorshidi G, Beckmann CF, et al. ICA-based artefact removal and accelerated fMRI acquisition for improved resting state network imaging. *Neuroimage*. 2014; 95: 232-47.
4. Burgess GC, Kandala S, Nolan D, et al. Evaluation of Denoising Strategies to Address Motion-Correlated Artifacts in Resting-State Functional Magnetic Resonance Imaging Data from the Human Connectome Project. *Brain connectivity*. 2016; 6: 669-80.
5. Abdallah CG, Averill CL, Salas R, et al. Prefrontal Connectivity and Glutamate Transmission: Relevance to Depression Pathophysiology and Ketamine Treatment. *Biol Psychiatry Cogn Neurosci Neuroimaging*. 2017; 2: 566-74.
6. Abdallah CG, Averill LA, Collins KA, et al. Ketamine Treatment and Global Brain Connectivity in Major Depression. *Neuropsychopharmacology*. 2017; 42: 1210-9.
7. Abdallah CG, Wrocklage KM, Averill CL, et al. Anterior hippocampal dysconnectivity in posttraumatic stress disorder: a dimensional and multimodal approach. *Translational psychiatry*. 2017; 7: e1045.
8. Murrough JW, Abdallah CG, Anticevic A, et al. Reduced global functional connectivity of the medial prefrontal cortex in major depressive disorder. *Hum Brain Mapp*. 2016; 37: 3214-23.
9. Anticevic A, Brumbaugh MS, Winkler AM, et al. Global prefrontal and fronto-amygdala dysconnectivity in bipolar I disorder with psychosis history. *Biol Psychiatry*. 2013; 73: 565-73.
10. Anticevic A, Corlett PR, Cole MW, et al. N-methyl-D-aspartate receptor antagonist effects on prefrontal cortical connectivity better model early than chronic schizophrenia. *Biol Psychiatry*. 2015; 77: 569-80.
11. Anticevic A, Hu S, Zhang S, et al. Global resting-state functional magnetic resonance imaging analysis identifies frontal cortex, striatal, and cerebellar dysconnectivity in obsessive-compulsive disorder. *Biol Psychiatry*. 2014; 75: 595-605.
12. Anticevic A, Hu X, Xiao Y, et al. Early-course unmedicated schizophrenia patients exhibit elevated prefrontal connectivity associated with longitudinal change. *J Neurosci*. 2015; 35: 267-86.
13. Cole MW, Anticevic A, Repovs G and Barch D. Variable global dysconnectivity and individual differences in schizophrenia. *Biol Psychiatry*. 2011; 70: 43-50.
14. Cole MW, Yarkoni T, Repovs G, Anticevic A and Braver TS. Global connectivity of prefrontal cortex predicts cognitive control and intelligence. *J Neurosci*. 2012; 32: 8988-99.
15. Driesen NR, McCarthy G, Bhagwagar Z, et al. Relationship of resting brain hyperconnectivity and schizophrenia-like symptoms produced by the NMDA receptor antagonist ketamine in humans. *Mol Psychiatry*. 2013; 18: 1199-204.
16. Driesen NR, McCarthy G, Bhagwagar Z, et al. The impact of NMDA receptor blockade on human working memory-related prefrontal function and connectivity. *Neuropsychopharmacology*. 2013; 38: 2613-22.

17. Liang X, Zou Q, He Y and Yang Y. Coupling of functional connectivity and regional cerebral blood flow reveals a physiological basis for network hubs of the human brain. *Proc Natl Acad Sci U S A*. 2013; 110: 1929-34.
18. Cole MW, Pathak S and Schneider W. Identifying the brain's most globally connected regions. *NeuroImage*. 2010; 49: 3132-48.
19. Glasser MF, Coalson TS, Robinson EC, et al. A multi-modal parcellation of human cerebral cortex. *Nature*. 2016; 536: 171-8.